

Using spatial derivatives of electromagnetic data to map lateral conductance variations in thin-sheet models: Applications over mine tailings ponds

Michal Kolaj¹ and Richard Smith¹

ABSTRACT

Mine waste, variable overburden, and the saprolite associated with nickel laterites have conductivity thicknesses (conductances) that vary laterally. In order for electromagnetic methods to be used to easily map lateral changes in conductance over thin-sheet-like bodies such as these, a simple conductance estimation method has been developed from Price's equation. Through forward modeling, we found that assuming a uniform conductance and solving for an apparent conductance was sensitive enough to identify lateral conductance changes. The method was independent of the transmitter location, and each measurement provided a direct estimate of the apparent conductance below that station. The receiver can be moved around quickly allowing for lateral variations in apparent conductance to be determined efficiently. However, one of the required terms in the equation used is the vertical derivative of the secondary vertical magnetic field (dH_z^s/dz). The accurate measurement of spatial

electromagnetic derivatives requires a good signal-to-noise ratio (S/N), which can be hampered by low derivative signal values. Field studies performed over a dry tailings pond in Sudbury, Ontario, Canada, showed that an S/N greater than three was achievable even with dH_z^s/dz values of less than 0.5 pT/(Am). Apparent conductance estimates revealed that the tailings had a large resistive zone associated with surface vegetation, which may be correlated with favorable growing conditions and/or less conductive or thinner tailing material. Larger apparent conductances in other areas may be related to zones of thicker tailings and/or more conductive material (possibly due to increased metal content). Further drilling and sampling work is required to answer these ambiguities. Regardless, mapping the conductance of a thin sheet is an important step toward assessing if there are leftover metals in mine waste. However, the developed method is general and can be used in many other situations involving laterally varying thin bodies.

INTRODUCTION

Mapping terrain with laterally varying conductivity using electromagnetic (EM) geophysical techniques is a potentially important step in characterizing mine waste, exploring over variable overburden, or characterizing the saprolite associated with nickel laterites. One way of simplifying the interpretation of these data is to use the thin-sheet approximation, which assumes that all the induced current is constrained to flow in the plane of the sheet (Grant and West, 1965). This assumption has proven to be effective in modeling and inversion because it allows for simplifications in the equations that describe the interactions between EM fields and the medium (Price, 1949; Grant and West, 1965; West et al.,

1984; Macnae and Lamontagne, 1987; Nabighian and Macnae, 1991; Smith, 2000; Swidinsky and Edwards, 2009).

However, variations in conductance (product of conductivity and thickness) within the sheet are often not considered, and many modeling routines do not allow for such variations, which is nonideal and may produce erroneous and/or misleading results in situations in which the thickness and/or conductivity of the sheet varies laterally. Such variations would be expected in exploration over variable overburden (Irvine and Staltari, 1984), nickel laterite exploration (Peric, 1981; Rutherford et al., 2001), or in the characterization of mine, mill, or smelter waste (Chouteau et al., 2006). EM induction in a thin sheet with laterally varying conductance obeys a differential equation derived by Price (1949). Smith and

Manuscript received by the Editor 30 October 2012; revised manuscript received 28 February 2013; published online 1 August 2013.

¹Laurentian University, Department of Earth Sciences, Sudbury, Ontario, Canada. E-mail: mx_kolaj@laurentian.ca; rsmith@laurentian.ca.

© 2013 Society of Exploration Geophysicists. All rights reserved.

West (1987) adapt the equation for EM prospecting and create a computational method to calculate the EM response of a sheet with variable conductance; however, no inversion based on this method has been developed. One of the terms in the equation is the vertical derivative of the secondary vertical magnetic field (dH_z^s/dz), termed the *vertical spatial derivative* henceforth. Spatial EM derivatives can be approximated with a finite-difference operator (using two sensors and taking the difference between their individual measurements). Because the difference in the field can be small, the sensors must be sensitive with low instrument noise levels.

Sattel and Macnae (2001) argue that spatial EM derivatives may offer increased resolution to the near-surface conductivity structure and provide noise reduction due to the cancellation of spatially homogenous ambient noise. However, the measurements are hampered by requiring very low nonspatially homogenous noise levels. The use of spatial magnetic field derivatives has seen notable research in magnetotelluric (MT) geophysics (Jones [1983]; Vozoff [1991]; Patella and Siniscalchi [1994], and the references therein), which is not surprising considering that the electric field used in the standard MT ratio (impedance) resistivity calculation (Vozoff, 1991) can be expressed in terms of spatial magnetic field derivatives via Ampere's law. Several EM gradiometer systems have also been developed for utility and tunnel detection (Bartel et al., 1997; McKenna et al., 2011), but little research has been undertaken in measuring and using spatial EM derivatives on the larger scales required for prospecting purposes.

One of the situations in which spatial EM derivatives should be measurable and in which a simple method to map lateral variations in conductance is useful is in the characterization of mine tailings. Tailings are the waste material produced after processing ore to extract valuable metals. The mine tailings waste dumps can be as large as several kilometers in length and several tens of meters in height and are found close to mines and mine-processing facilities. The processing techniques used to remove the metals of interest from the original rock are not completely effective even today, and certainly they were not more than 100 years ago when some of these tailings were first produced (Brown et al., 1999; Marcuson and Diaz, 2007). Thus, the older mine tailings may contain metal concentrations that, by today's standards, may be economical to extract, and reprocessing them may prove to be an alternate source of easy-to-access metals (Xie et al., 2005). As such, delineating the electrical properties of mine tailings may aid in identifying zones of high concentrations of metals (Chouteau et al., 2006; Lacob and Orza, 2008; Martinez-Pagan et al., 2009; Anterrieu et al., 2010). Furthermore, because some mine tailings are generally quite fine to powdery in consistency, the metals can seep into the surface and subsurface water, and thus their characterization is also important from an environmental standpoint (Aplin and Argall, 1973; Akcil and Koldas, 2006). Finding the metals and reprocessing them will reduce the potential for seepage in the future. The EM geophysical data may not be able to distinguish between enhanced conductance due to changes in thickness or conductivity and increased clay, water, or metal content. However, these ambiguities can be solved through drilling and sampling work on areas of interest identified by the geophysical work.

In this paper, the solution to the problem of EM induction in laterally varying thin sheets is simplified to require only two measured quantities from which the conductance of the sheet can be calculated. In addition, forward modeling is used to generate typical

apparent conductance results at various conductances. Lastly, we present results from field data collected atop a laterally extensive dry mine tailings pond (variably covered by vegetation and hay) situated on Vale property in Sudbury, Ontario, Canada, where the vertical spatial derivative of the magnetic field was measured during an inductive time-domain EM (TDEM) survey.

THEORY

In the thin-sheet approximation, the sheet's thickness is considered small enough such that the current density induced in the sheet by the exciting primary magnetic field \mathbf{H}^P is constrained to flow in the plane of the sheet (i.e., no current flow normal to the sheet; Price, 1949). Such a sheet is often referred to as being *inductively thin*. This condition is valid as long as the thickness of the sheet is smaller than one-half the skin depth in the frequency domain or the diffusion depth in the time domain (Joshi et al., 1988; Frischknecht et al., 1991). This approximation allows for a reasonably simple relationship between the secondary magnetic field \mathbf{H}^S and the total magnetic field \mathbf{H} (i.e., $\mathbf{H}^P + \mathbf{H}^S$) to be derived for a flat-lying thin sheet in a nonconductive medium (Price, 1949; Smith and West, 1987):

$$-\frac{dH_z^s}{dz}R + \frac{dR}{dy}H_y^s + \frac{dR}{dx}H_x^s = -\frac{\mu}{2} \frac{dH_z}{dt}, \quad (1)$$

where μ is the magnetic permeability; $R(x, y)$ is the resistance of the sheet (the resistance directly below the measurement point (x, y)); and the variables dH_z^s/dz , H_y^s , H_x^s , and dH_z/dt are measured above the sheet. As a result of having a vanishing thickness, the sheet is represented by a single parameter, the resistance (product of resistivity and thickness, inverse of conductance) rather than two parameters, the resistivity and thickness. As such, in realistic scenarios in which the sheet has a thickness but the thin-sheet approximation is still valid, the thickness and resistivity information is incorporated into the resistance value.

Equation 1 can be simplified if we assume that the sheet is infinite in extent and that the resistance is constant in the x - and y -direction, i.e., set dR/dy and dR/dx equal to zero such that equation 1 reduces to

$$\frac{dH_z^s}{dz}R = \frac{\mu}{2} \frac{dH_z}{dt}. \quad (2)$$

If the vertical spatial derivative dH_z^s/dz and the vertical component time derivative dH_z/dt are sensitive to lateral changes in resistance and the terms with resistance derivatives in the lateral direction in equation 1 are very small (i.e., $H_y^s dR/dy \approx 0$ and $H_x^s dR/dx \approx 0$), then equation 2 can also be used to estimate the "apparent resistance" in sheets in which the resistance varies laterally. This apparent resistance assumes a thin-sheet model with a uniform resistance (equation 2) in the same way that apparent resistivity in the DC resistivity method normally assumes a uniform half-space model. If viable, this simplification implies that laterally varying resistance could be determined experimentally (or analytically) at each location by measuring only the vertical component of the magnetic field at two heights. Only one transmitter would be required (either on the ground or in the air), and the receiver could be moved around quickly allowing for lateral variations in apparent

resistance to be determined efficiently using equation 2. A further simplification can be achieved by making equation 2 independent of the transmitter properties (location and waveform) by setting dH_z^p/dt equal to zero (all terms become secondary magnetic fields). This is true in the off time or when the transmitted waveform has a constant valued magnetic field (i.e., $dH_z^p/dt = 0$). Furthermore, because there is no explicit dependence on time in equation 2, multiple resistance profiles can be calculated, one for each time channel. The apparent resistance calculated using different time channels should be equal if the inductively thin sheet and uniform resistance approximations are valid. Similarly, equation 2 has no explicit dependence on depth, but dH_z^s/dz will inherently limit the applicability of this method for non-near-surface targets as dH_z^s/dz from deeper targets will become obscured in background noise levels. Lastly, in this study, the magnetic permeability μ is set to be that of free-space (nonmagnetic material) but it may be possible in future work to include variability in μ to map magnetic permeability variations in addition to resistance.

A method to estimate the subsurface resistance using the thin-sheet approximation is not a new endeavor, but estimating the resistance using equation 1 (or the simplified version, equation 2) has not been done previously. This is likely due to the potentially problematic measurement of the vertical spatial derivative. Furthermore, unlike the approach presented here, other methods generally involve using some form of inversion, which is considerably more difficult to solve (Keating and Crossley, 1990; Liu and Asten, 1993).

FORWARD MODELING

In this section, we test the idea of using the equation that describes the EM induction in thin sheets with a constant resistance (equation 2) on models with laterally varying resistance. The forward modeling was performed using MultiLoop III (Lamontagne Geophysics, Walker and Lamontagne, 2006).

A simple nonuniform resistance case can be represented by a small circular feature in the center of a large sheet (pseudoinfinite). A two-magnetic-field sensor ground survey (to measure the vertical spatial derivative with a 2-m sensor separation) with a 30-Hz 100% duty periodic square wave transmitted waveform was simulated in MultiLoop III for the model shown in Figure 1. The time channels were measured over 10 windows spaced in a binary geometric progression (common ratio of 2, West et al., 1984). The data from this were used to solve for the resistance using equation 2 (simplified method) to produce Figures 2 and 3. The survey was simulated inside of the transmitter loop (Tx loop, Figure 1) because this was found to give the best results given that the vertical magnetic field is the largest in this layout (i.e., increases the likelihood that the ignored terms in equation 1 are small).

Because the modeled data provide the vertical magnetic field (H_z^s) averaged over several time intervals (windows or channels) at two heights, the vertical spatial derivative dH_z^s/dz was calculated by using the difference in the H_z^s field at these two heights (Figure 2a). Because dH_z^p/dt is equal to zero everywhere, apart from where the current changes polarity, the vertical component time derivative (dH_z/dt) was calculated by taking a forward difference between adjacent channels (Figure 2b). Because the time derivative was calculated by using two adjacent channels, the vertical derivative was averaged over the same two adjacent channels. If the time derivative (Figure 2b) is divided by the vertical derivative (Figure 2a) and multiplied by $\mu/2$, the apparent model resistance is

calculated (Figure 2c). Because each time channel can be used in equation 2, multiple resistance profiles can be calculated, one for each set of adjacent time channels. Note the increased resolution to the anomalous zone with dH_z^s/dz and how the apparent resistance anomaly is more strongly a function of dH_z^s/dz than dH_z/dt . Although equation 2 is independent of the time channel used, each time channel produces slightly different apparent resistances. Despite this, the background resistance of the sheet and the dimension of the anomaly are estimated to be 0.1 ohm and about 80–100 m in diameter, respectively, which are consistent with the input values. The resistance of the anomaly was overpredicted at an approximate resistance of 0.08–0.03 ohm versus the input model resistance of 0.01 ohm.

The method can be further tested using a variety of resistance contrasts. Figure 3 uses the survey geometry seen in Figure 1 with

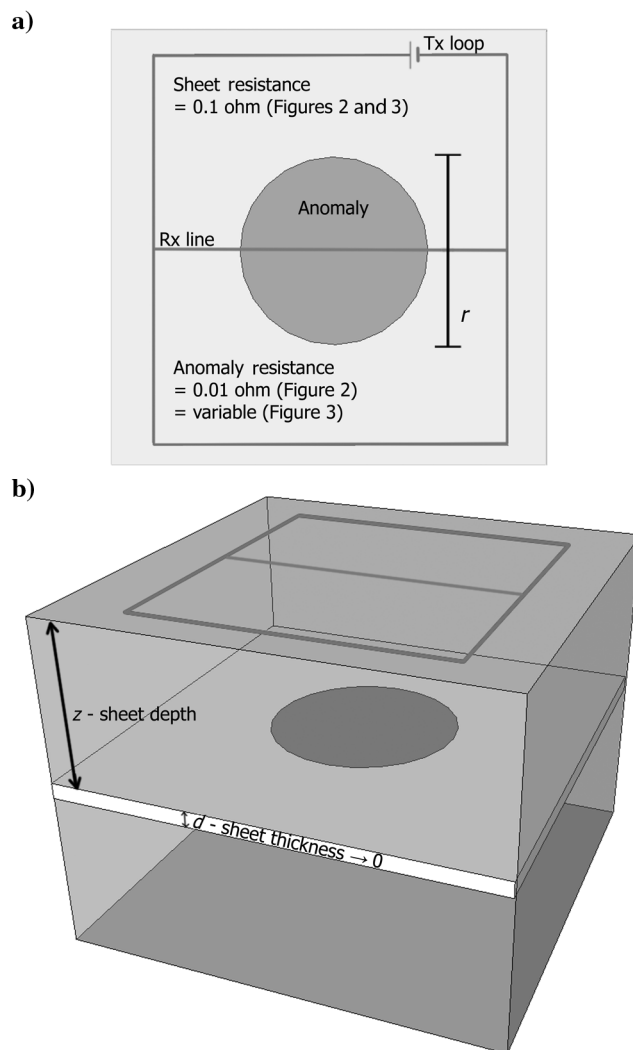


Figure 1. (a) Plan view and (b) oblique view of the generalized survey geometry and model used to produce the forward models in Figures 2 and 3 using MultiLoop III. Tx and Rx stand for transmitter and receiver, respectively. The sheet is at a depth (z) of 30 m, the background sheet resistance is 0.1 ohm, the diameter of the anomaly (r) is 80 m and 180 m for Figures 2 and 3, respectively, and the dark-gray circle represents the zone of anomalous resistance within the sheet. Model is not to scale.

a 400×400 -m transmitter loop, background resistance of 0.1 ohm, and with a varying resistance for the circular anomaly (0.01 ohm, 0.05 ohm, 0.5 ohm and 1 ohm). Figure 3a, 3b, and 3c shows the estimated apparent resistance at early, intermediate, and late time channels, respectively. For reference, a constant resistance model (i.e., no anomaly) is also shown (solid line). The same pattern as in Figure 2 is seen. Note that in Figure 3c, the most conductive contrast (0.01 ohm) generates negative results in the late-time response (which cannot be shown in the log plot). This is likely a function of the magnetic field strength at later times being significantly diminished allowing for numerical noise to be more pronounced. Forward modeling has revealed that although the calculated resistance of the anomaly is underpredicted for resistive anomalies or overpredicted for conductive anomalies (a common problem in estimating conductivity from EM data due to the lack

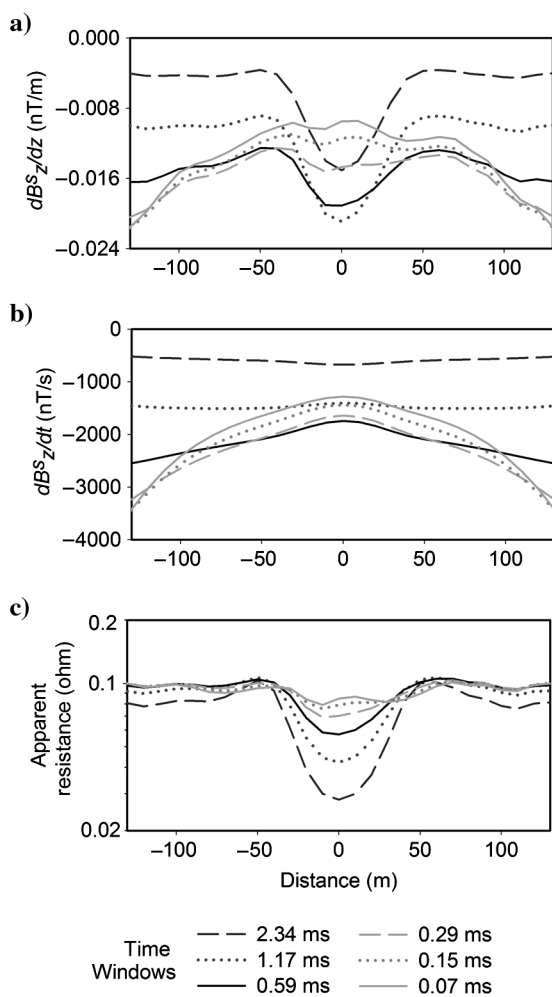


Figure 2. Forward model corresponding to a synthetic survey using the survey geometry seen in Figure 1 (500×500 -m transmitter loop, background and anomaly resistance of 0.1 and 0.01 ohm, respectively). (a) Vertical spatial derivative, (b) time derivative of the vertical magnetic field, and (c) apparent resistance calculated using equation 2. The different curves represent apparent resistance calculations using different sets of time channels. Note that the \mathbf{B} rather than \mathbf{H} magnetic fields are shown in this and subsequent figures because \mathbf{B} -field units (nT) are more commonly used in practice ($\mathbf{B} = \mu\mathbf{H}$).

of sensitivity of the EM response to changes in the resistivity of highly resistive and/or small features), it is in the correct sense (more or less resistive than the background), and its spatial dimensions are well defined.

Two potential adverse side effects emerge from using an infinite sheet and uniform resistance assumption on models that are finite in size and/or laterally varying. They are the under- or overprediction of the input model resistance and the disagreement between the resistances calculated using each set of time channels (Figure 3). They arise from the fact that each time channel corresponds to a different sampled area (due to the nature of the diffusing currents); the later in time, the larger the diffused current system. As such, each time channel may invalidate the method's assumptions (infinite, inductively thin, and uniform resistance) differently. Changing the depth of the sheet will have a similar effect on the apparent resistance calculated because the established current systems will be different. The calculated resistance in Figures 2 and 3 are progressively smaller toward the later time channels because these channels are associated with currents that are impacted by the edge of the sheet. The difference is not as pronounced in more conductive models

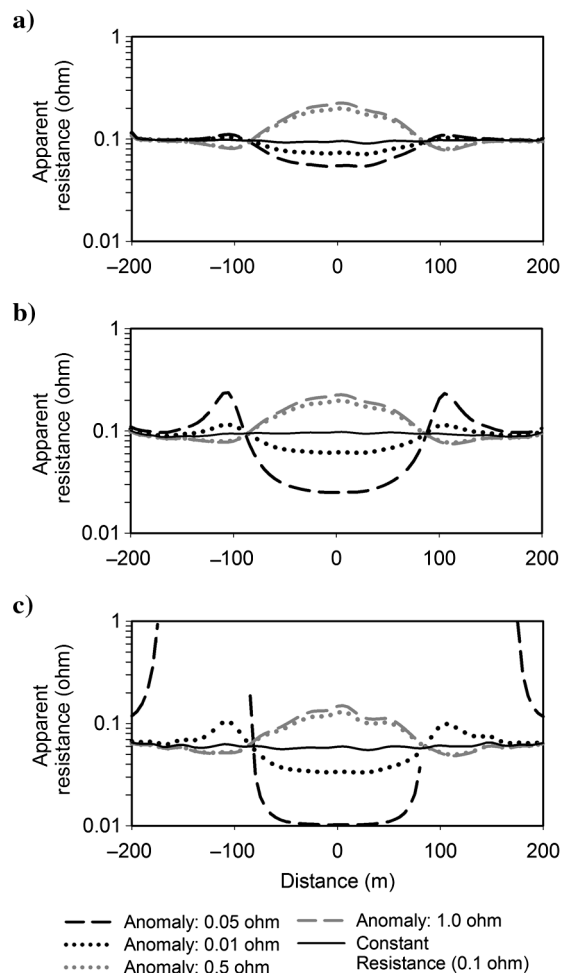


Figure 3. Apparent resistance calculated using equation 2 for synthetic models corresponding to surveys using the survey geometry seen in Figure 1 (400×400 -m transmitter loop) at various resistance contrasts and various time channels. (a) Early time, (b) intermediate time, and (c) late time.

because the currents do not diffuse as quickly. It is important to use all of the available time channels because they may be sensitive to different areas within the sheet, and by investigating the resistance calculated at each set of time channels, it may be possible to estimate the size of the sheet and/or the resistivity with depth.

FIELD DATA

A shallow and laterally extensive dry mine tailings pond situated on Vale property in Sudbury, Ontario, Canada, should be possible to model as an inductively thin sheet because its small thickness should satisfy the thin-sheet approximation criteria. It is also suspected to contain a laterally varying resistance as is sometimes found in waste rock piles (Chouteau et al., 2006). The resistance variations may be due to changes in the thickness of the tailing based on the underlying topography of the ground (which was unknown) or due to conductivity variations as a result of the dumping of different material over the lifespan of the tailings pond. A Geonics EM34-3 survey was first performed to obtain an independent data set to which the results from equation 2 could be compared. See Figure 4 for the station locations for the EM34-3 (open squares) and dH_z^e/dz TDEM (closed circles) surveys and

the TDEM transmitter loop location (dashed line). The shape of the transmitter loop is largely a result of the ground conditions and the desire to minimize transmitter noise by placing the loop edges further from the survey lines.

Geonics EM34-3

The EM34-3 survey was carried out over four lines spaced 40 m apart with stations every 20 m and an additional three stations spaced 40 m apart centered between each of the lines (Figure 4). The sensors were located directly on the ground, and the transmitter-receiver offset was held at a constant 10 m and was operated in horizontal and vertical dipole mode to provide effective depths of exploration of 7.5 and 15 m, respectively. A two-layer model (tailing and basement) with a basement conductivity of 0 S/m was assumed (reasonable assumption for the area). This resulted in two equations (one for each dipole mode) with two unknowns (conductivity and thickness) using the formulas found by McNeill (1980). This system of equations was solved, and the conductance of the tailings pond was calculated from the product of the conductivity and thicknesses (Figure 5). The high values of conductance to the northwest are likely to be the result of a large pipe or a road running from north to south along the western edge of the survey

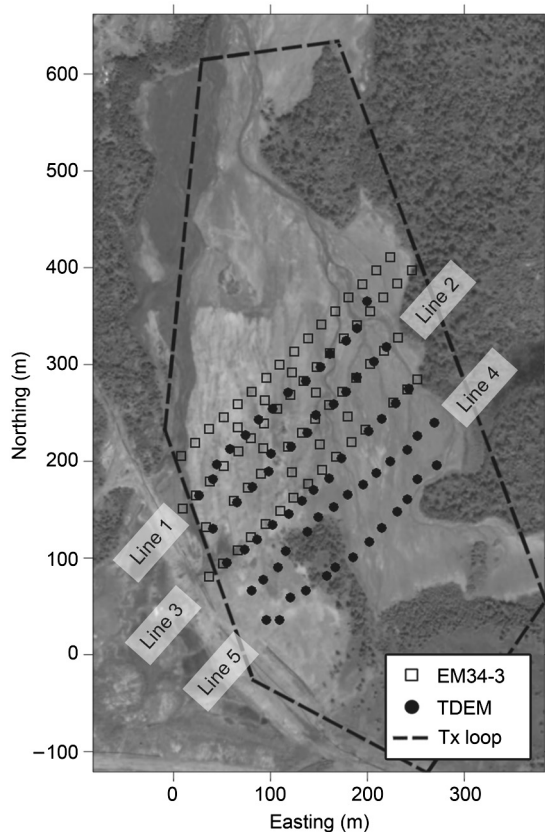


Figure 4. Station locations for the Geonics EM34-3 and vertical spatial derivative TDEM surveys superimposed atop an aerial image of the dry tailings pond on Vale property located in Sudbury, Ontario, Canada. The lines indicated (e.g., “Line 1”) are for the TDEM survey. Open squares are the locations for the EM34-3 survey, closed symbols are for the TDEM receiver locations, and the black dashed line represents the approximate location of the transmitter loop for the TDEM survey.

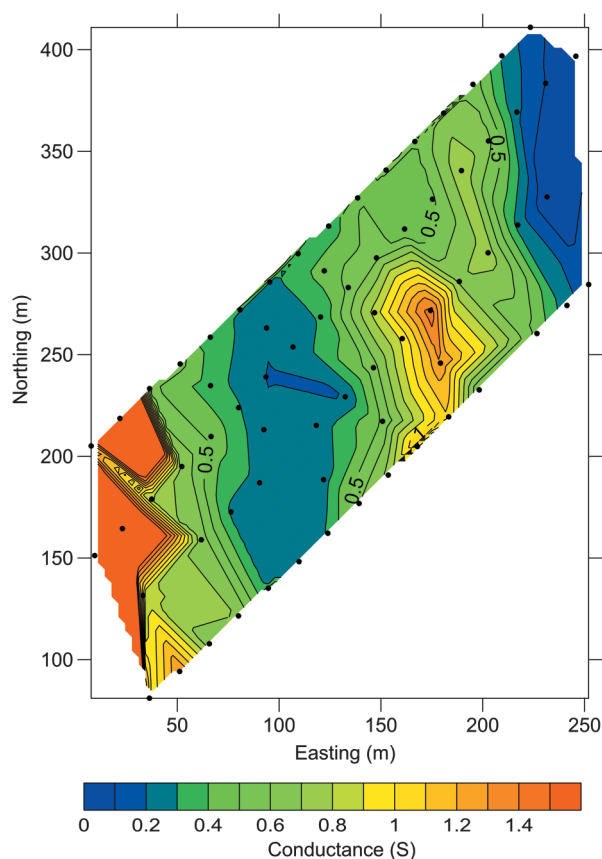


Figure 5. Contoured conductance over the dry tailings pond calculated by assuming a two-layer case with the bottom layer having a conductivity of 0 S/m. Survey data were acquired using the Geonics EM34-3 at a transmitter-receiver separation of 10 m. Black dots represent station locations. Gridding on this and subsequent figures used triangulation with linear interpolation.

area. Therefore, the general observed pattern can be thought of as a conductive area in the center with a resistive area along the edges.

TDEM survey

The TDEM survey was performed inside of a loop roughly 700×350 m with a 30-Hz 50% duty cycle exponential turn on linear ramp off waveform generated using a Geonics TEM-57 transmitter. The transmitter is not identical to the one tested in the forward modeling section, but it should produce the same results because in both cases, dH_z^p/dt is equal to zero, making equation 2 independent of the transmitter. A SMARTem24 receiver was used with Geonics 3D-3 sensor coils measuring the horizontal (x and y , inline, and crossline, respectively) and vertical (z) components. Three 3D-3 coils were located on three different platforms spaced vertically apart by 1.1 m. In addition to the Geonics sensors, three vertical feedback coils (magnetometers) were also used; however, their use is not relevant to this paper. The structure that held these sensors was composed entirely of PVC pipe and wood (Figure 6). In this experiment, the prototype structure was designed to be dragged along a clear opening atop snow, but similar structures could be designed to meet specific requirements. The survey was performed over five lines spaced 40 m apart with stations every 20 m along the line. The southern three lines of the Geonics EM34-3 survey corresponded approximately to lines 1–3 in this survey (Figure 4).

Each station measurement included five readings of about 30 s (756 stacks), and the sensor coil output was proportional to the time



Figure 6. Vertical spatial derivative measurement structure made of PVC pipe and wood housing three Geonics 3D-3 coils (x , y , and z components) and three vertical B-field feedback sensors with each level separated by 1.1 m. The apparatus was dragged from station to station.

derivative of the magnetic field ($dB_x/dt, dB_y/dt, dB_z/dt$). This was integrated to give the magnetic field (B_x, B_y, B_z) using the full waveform data (Smith and Annan, 2000). The data were then windowed and averaged (B_z and B_x at the base level coil can be seen in Figures 7 and 8, respectively). The crossover in the B_z component and the peak in the B_x component (trending northwest–southeast) are suggested to be caused by the edge of the conductive portion of

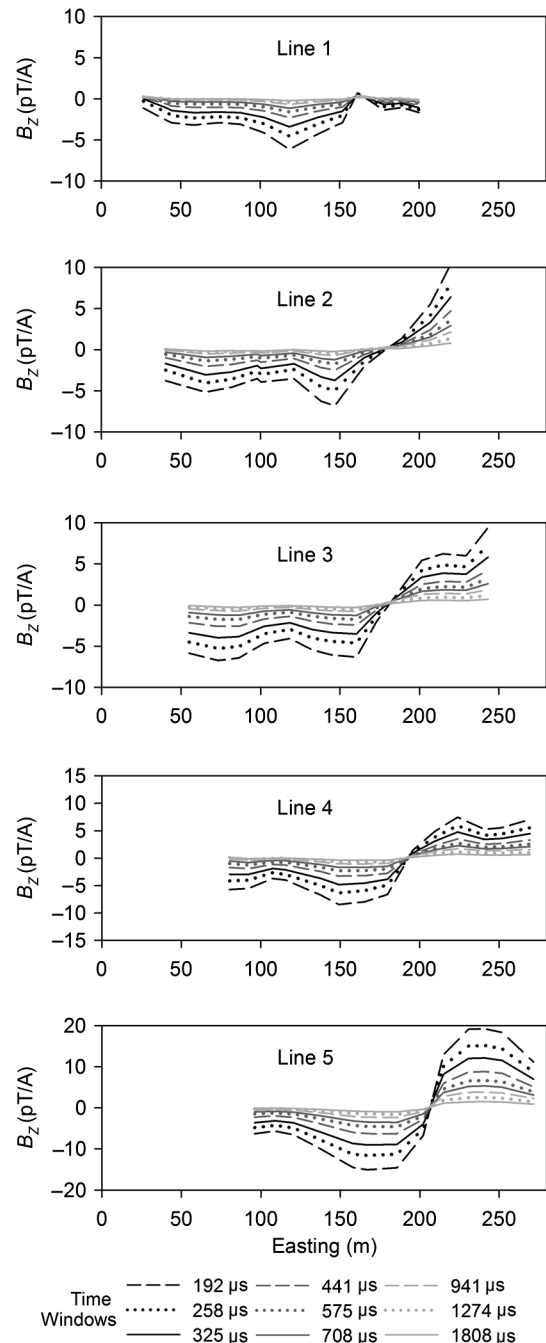


Figure 7. Off-time, integrated, windowed, and stacked B_z for the base-level Geonics coil. The quantity measured is the magnetic field integrated from the measured voltage. Noise estimates were found to range from approximately 0.01–0.1 pT/A (mean of 0.04 pT/A for all three sensors).

the tailings pond. Noise estimates, calculated by taking the standard deviation between five stacked and windowed waveforms, were found to range from approximately 0.01–0.1 pT/A (mean of 0.014 pT/A) for the vertical components. The vertical spatial derivative (dH_z^s/dz) was obtained by calculating the vertical derivative using the difference between the base and the average of the mid and upper sensors because this combination had the lowest noise (Figure 9). As would be expected by taking a spatial deriva-

ive, many of the subtle changes along the profiles in Figure 7 are more pronounced in Figure 9. For reference, a thick black line is used to indicate the noise levels averaged over the first five windows (mean of 0.03 pT/(Am)). The signal-to-noise ratio (S/N) (relative error, Figure 10) for window 1 ($t = 192 \mu\text{s}$) is, on average, well below 33% (larger over lines 2 and 3 and where the signal is very

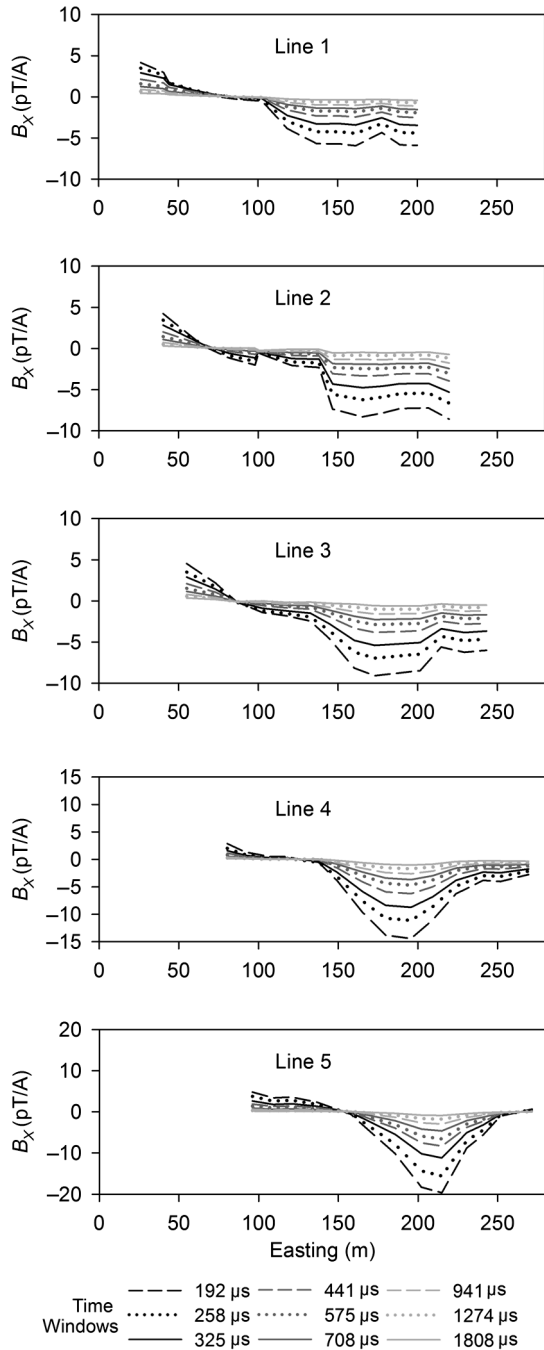


Figure 8. Off-time, integrated, windowed, and stacked B_x (inline) for the base level Geonics coil. The quantity measured is the magnetic field integrated from the measured voltage.

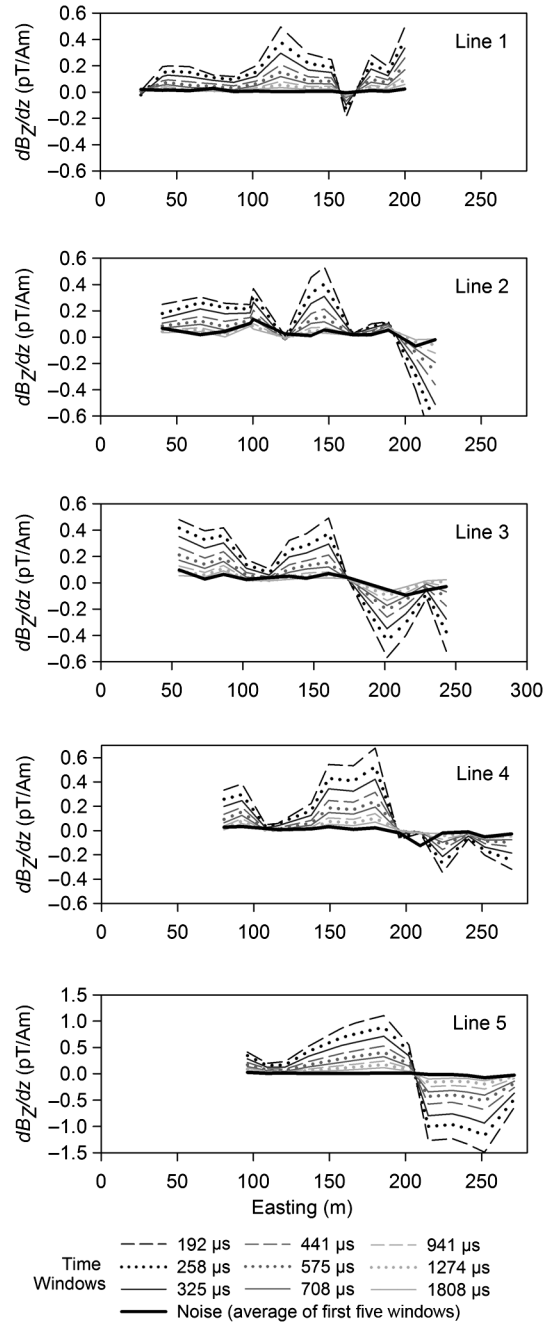


Figure 9. Off-time, integrated, windowed, and stacked vertical spatial derivative (dB_z/dz) calculated from the difference between the base and the average of the mid and upper sensors. The thick black line is used to indicate the noise levels averaged over the first five windows (mean of 0.03 pT/(Am)). The vertical spatial derivative is visibly above the noise levels for the early windows.

low), which provides an adequate S/N on which equation 2 can be tested.

APPARENT CONDUCTANCE RESULTS

Because equation 2 was developed to be used over a thin-sheet model, any stations not located atop the sheet were removed because they violate the inherent assumptions (stations to the right of the crossover in B_z). Furthermore, all stations with an S/N below 3 were also removed (Figure 10). The apparent resistance was calculated using equation 2, and the apparent conductance (inverse of apparent resistance) for early and intermediate time can be seen in Figure 11. The relative error in the apparent conductance (Figure 12) was on average less than 10% (larger over interpreted resistive zones and where dH_z^2/dz noise levels were increased).

The general observed pattern in Figure 11 in the early time ($t = 192 \mu\text{s}$) is a southwest–northeast-trending resistive zone to the south and a southwest–northeast-trending conductive zone to the north. The intermediate time ($t = 575 \mu\text{s}$) results are roughly twice as conductive and are dominated by a south–north-trending resistive zone. The increase in apparent conductance with time is also evident in the synthetic data and, as argued above, may be a result of the finite size of the tailings pond. Variations in apparent conductance (at each delay time) may be due to changes in the tail-

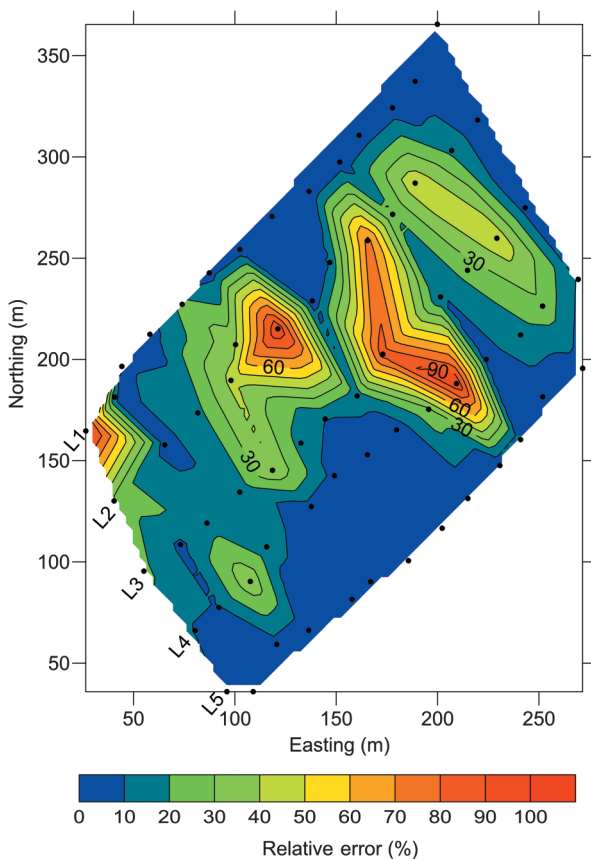


Figure 10. An S/N map (relative error) calculated for window 1 ($t = 192 \mu\text{s}$) of Figure 9. Line numbers are indicated, and black dots represent station locations. Note that where the relative error exceeded 100%, a value of 100% was assigned to allow the full range of data to be seen.

ing thickness or due to conductivity variations from factors such as particle size variations, water content, and/or the presence of electrically conductive metals (Telford et al., 1990; Samouelian et al., 2005; Martinez-Pagan et al., 2009). Because the resistive zone to

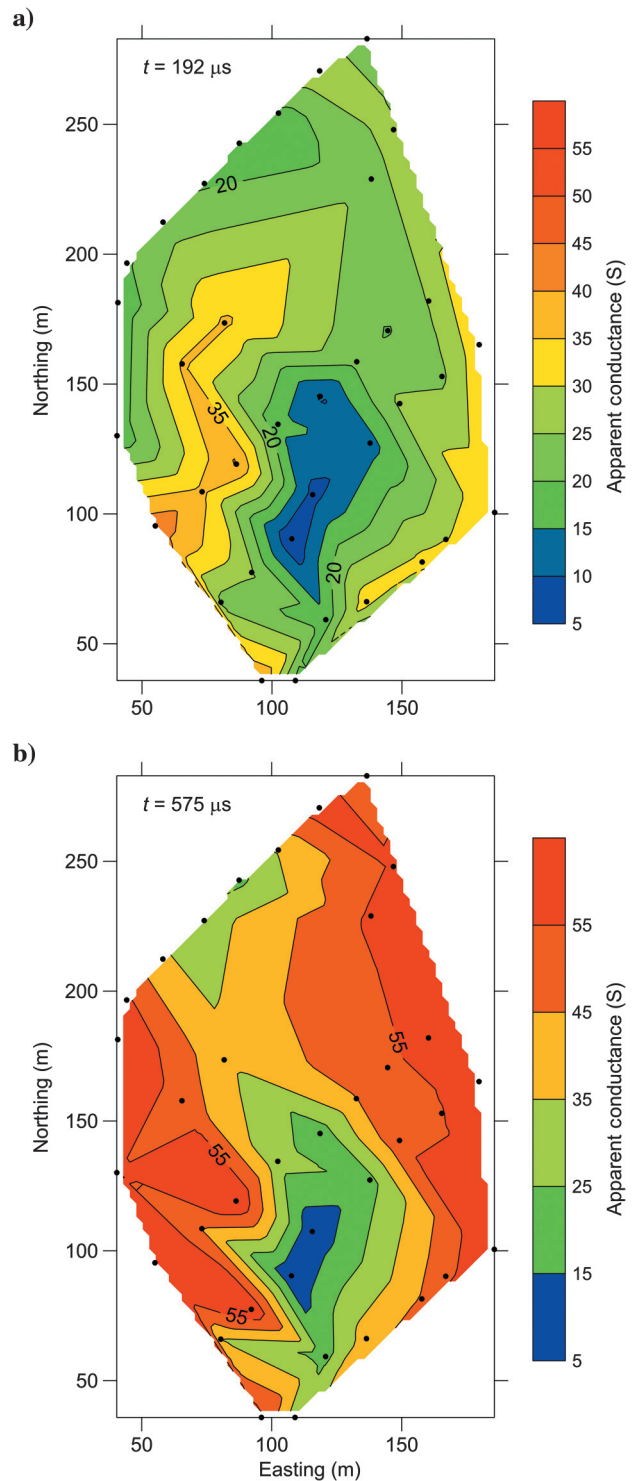


Figure 11. Apparent conductance over the tailings pond calculated using equation 2 for (a) early time (window 1) and (b) intermediate time (window 5). Black dots represent station locations.

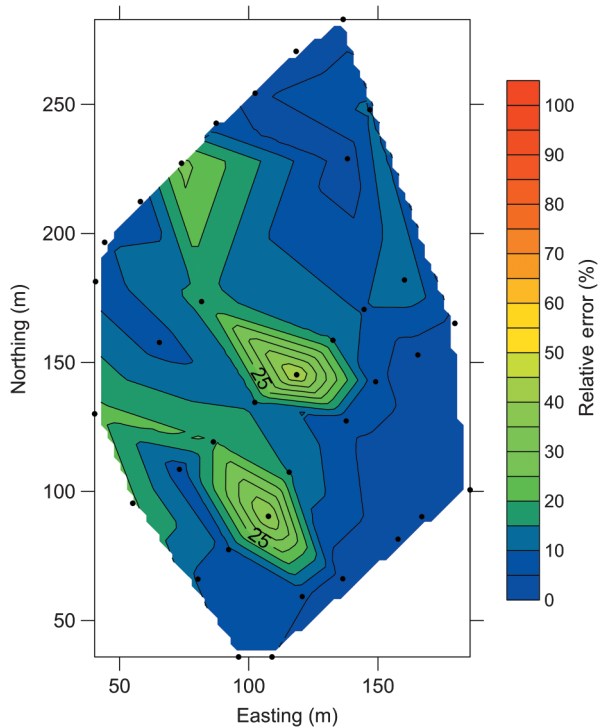


Figure 12. A relative error map calculated for the early time window conductance calculation in Figure 11. The relative error is, on average, 10%. Black dots represent station locations.

the south roughly matches the location of a more vegetated area (Figure 4), there may be a link between the ability of the tailings to support vegetation and areas of low conductance (i.e., thinner waste or less conductive material). In contrast, the zones with a higher conductance may represent more conductive areas due to increased metal concentrations and/or thicker portions of tailings.

The similarity in the shape of the zones in the EM34-3 conductance and equation 2 conductance estimates (Figure 13) include an interpreted resistive zone running roughly through the middle of the area with more conductive zones on either side. The continuity of this resistive zone in the early time results may have been more intact and similar to that of the late time or EM34-3 estimate had the S/N along the middle of line 2 been higher. The major difference between them is that the EM34-3 conductance estimates are significantly lower than that calculated using equation 2. It is possible that this discrepancy is due to the two methods imaging different depths of the tailings pond. The EM34-3 had a depth of penetration of less than 20 m, whereas the TDEM survey suggests a body that is much deeper based on the breadth of the anomalies (the peak-to-peak distance around the crossover). As such, it is suggested that the EM34-3 survey imaged the near surface, which appears to be more resistive, and the developed methodology was more sensitive to a deeper and more conductive portion of the tailings pond.

The apparent conductance estimates changing with delay time are also consistent with the hypothesis that the conductivity or conductance structure of the tailings changes with depth. Additionally, the EM34-3 conductance estimate was based on the assumption of a two-layer model with the bottom layer having a conductivity of zero, which may be untrue considering that the TDEM survey suggests a deeper conductor. Furthermore, the EM34-3 apparent conductivity readings rely on a low-induction number assumption, which breaks down as the conductivity is increased (McNeill, 1980). For these reasons, equation 2 may be a more reliable and accurate mapping technique than the EM34-3. Another possible reason for the discrepancy is that our thin-sheet assumption or assumption that the product of the spatial derivatives of resistance and the corresponding horizontal magnetic field is small may be incorrect. Mutual coupling effects between the sensors were also assumed to be negligible, and if present, they may have introduced some error into the apparent conductance estimation.

CONCLUSION AND FUTURE WORK

The differential equation that describes induction in a thin sheet with laterally varying resistance can be simplified to require only two measurable quantities: dH_z^2/dz and dH_z/dt . Through forward modeling, we showed that the simplified differential equation can accurately determine an apparent resistance at specific locations above thin-sheet models in which the resistance is not uniform. Mapping conductance as a function of lateral position in a thin-sheet model is an important step toward assessing if there are leftover metal concentrations in mine waste. In real field data, collected

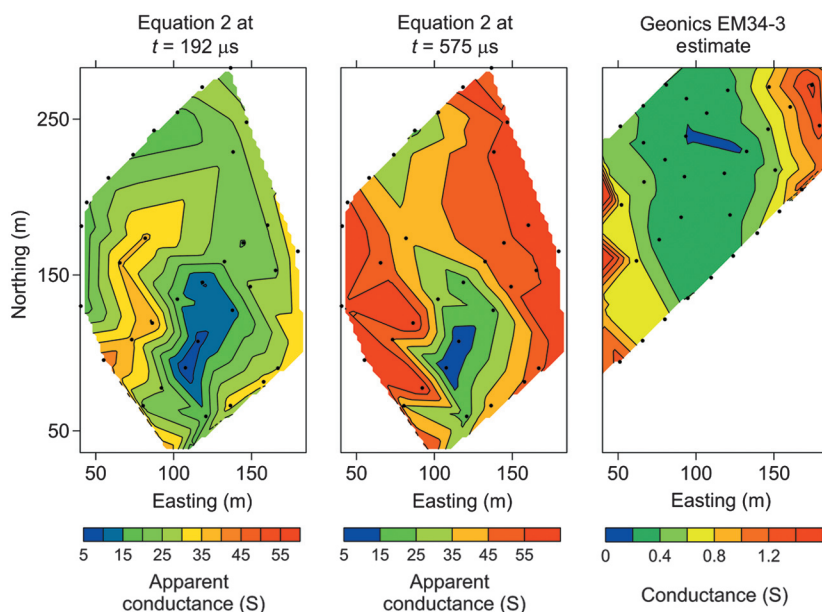


Figure 13. Comparison of Figure 11 (apparent conductance estimate using the developed method, equation 2) and Figure 5 (conductance estimate using the Geonics EM34-3 system) scaled to the same map limits. Black dots represent station locations. A resistive zone runs through the middle of each conductance estimate.

atop a dry tailings pond dH_z^2/dz is small, but above the noise levels. Apparent conductance estimates using the developed methodology revealed that the dry tailings pond has zones of varying conductance and a large resistive zone associated with surface vegetation. Further work would be required to determine whether zones in which the conductance is low are correlated with thinner and/or less conductive tailing material and whether zones of greater conductance (areas in which there is no vegetation) are related to zones of increased metal (or even clay) concentrations and/or thicker tailings. The geophysical data can be used to guide a sampling program that would answer these ambiguities.

Even though this field example was on a dry tailings pond, the methodology is general and could be used to estimate an apparent conductance over any thin-sheet-like body such as for estimating overburden conductance and for nickel laterite exploration and characterization. Hence, we believe that mapping a laterally varying conductance using the derived equation can be practically performed and be of benefit.

Future work involves developing a way to transform the conductance data into conductivity versus depth; forward modeling of the response over the dry tailings pond; and developing, testing and comparing the full equation (i.e., addition of the terms involving the product of the resistance derivatives with the horizontal magnetic fields) to the simplified approach presented here.

ACKNOWLEDGMENTS

We are grateful to the following for financial support of this research: NSERC, Vale, Xstrata Nickel, Wallbridge Mining, KGHM International, and CEMI. M. Kolaj is grateful for an NSERC Alexander Graham Bell scholarship, an SEG/ARCO scholarship, and a KEGS/Fugro scholarship. We are also thankful to Abitibi Geophysics, in particular, R. Wasylechko, P. Berube, J. Collins, and E. Gilbert, who supplied assistance, equipment, and personnel that allowed for the field data to be collected. Thanks also to C. Samson of Carleton University and J. Lyburner of Laurentian University for their assistance with the field work and the Vale staff who were very helpful in assisting with the logistics, acquisition, and processing of the field data, in particular, G. McDowell, J. Repas, K. O'Neill, B. Polzer, A. Mackie, and S. Kant. MultiLoop III was provided by Lamontagne Geophysics, and P. Walker guided us in its use.

REFERENCES

- Akcil, A., and S. Koldas, 2006, Acid mine drainage (AMD): Causes, treatment and case studies: *Journal of Cleaner Production*, **14**, 1139–1145, doi: [10.1016/j.jclepro.2004.09.006](https://doi.org/10.1016/j.jclepro.2004.09.006).
- Anterrieu, O., M. Chouteau, and M. Aubertin, 2010, Geophysical characterization of the large-scale internal structure of a waste rock pile from a hard rock mine: *Bulletin of Engineering Geology and the Environment*, **69**, 533–548, doi: [10.1007/s10064-010-0264-4](https://doi.org/10.1007/s10064-010-0264-4).
- Aplin, C. L., and G. O. Argall, 1973, Tailing disposal today: *Proceedings of the First International Tailing Symposium*, Miller Freeman Publications Inc.
- Bartel, C. L., H. D. Cress, and G. L. Stolarczyk, 1997, Evaluation of the electromagnetic gradiometer concept for detection of underground structures — Theory and application: *Journal of Environmental and Engineering Geophysics*, **2**, 127–136, doi: [10.4133/JEEG2.127](https://doi.org/10.4133/JEEG2.127).
- Brown, D. G., K. J. DeVos, G. Hall, and B. Macnamara, 1999, Characterization of slag produced at the Falconbridge Limited smelter site: *Proceedings of Sudbury '99 Mining and the Environment II*, **2**, 755–764.
- Chouteau, M., O. Anterrieu, M. Aubertin, C. Dubreuil-Boisclair, and J. Poisson, 2006, Geophysical characterization of an AMD-generating waste rock pile using ground and borehole techniques: *Proceedings of the 19th EGS Symposium on the Application of Geophysics to Engineering and Environmental Problems*, Environmental and Engineering Geophysical Society, 128–139.
- Frischknecht, F. C., V. F. Labson, B. R. Spies, and W. L. Anderson, 1991, Profiling methods using small sources, in M. N. Nabighian, ed., *Electromagnetic methods in applied geophysics: Applications, Parts A and B*, vol. 2, *Investigations in Geophysics 3*: SEG, 105–270.
- Grant, F. S., and G. F. West, 1965, *Interpretation theory in applied geophysics*: McGraw-Hill.
- Irvine, R. J., and G. Staltari, 1984, Case history illustrating problems in transient electromagnetic surveys: *Exploration Geophysics*, **15**, 155–167, doi: [10.1071/EG984155](https://doi.org/10.1071/EG984155).
- Jones, A. G., 1983, A passive natural-source twin-purpose borehole technique: Vertical gradient magnetometry (VGM): *Journal of Geomagnetism and Geoelectricity*, **35**, 473–490, doi: [10.5636/jgg.35.473](https://doi.org/10.5636/jgg.35.473).
- Joshi, M. S., O. P. Gupta, and J. G. Negi, 1988, On the effects of thickness of the half-plane model in HLEM induction prospecting over sulphide dykes in a highly resistive medium: *Geophysical Prospecting*, **36**, 551–558, doi: [10.1111/j.1365-2478.1988.tb02179.x](https://doi.org/10.1111/j.1365-2478.1988.tb02179.x).
- Keating, P. B., and D. J. Crossley, 1990, The inversion of time-domain airborne electromagnetic data using the plate model: *Geophysics*, **55**, 705–711, doi: [10.1190/1.1442882](https://doi.org/10.1190/1.1442882).
- Lacob, C., and R. Orza, 2008, Integrated interpretation of geophysical data on metalliferous mining waste deposits: Presented at Near Surface 2008 — 14th European Meeting of Environmental and Engineering Geophysics, B02.
- Liu, G., and M. Asten, 1993, Conductance — Depth imaging of airborne TEM data: *Exploration Geophysics*, **24**, 655–662, doi: [10.1071/EG993655](https://doi.org/10.1071/EG993655).
- Macnae, J. C., and Y. Lamontagne, 1987, Imaging quasi-layered conductive structures by simple processing of transient electromagnetic data: *Geophysics*, **52**, 545–554, doi: [10.1190/1.1442323](https://doi.org/10.1190/1.1442323).
- Marcuson, W. S., and C. M. Diaz, 2007, The changing Canadian nickel smelting landscape — Late 19th century to early 21st century: *Canadian Metallurgical Quarterly*, **46**, 33–46, doi: [10.1179/000844307794535687](https://doi.org/10.1179/000844307794535687).
- Martinez-Pagan, P., A. Faz Cano, E. Aracil, and M. A. Arocena, 2009, Electrical resistivity imaging revealed the spatial properties of mine tailing ponds in the Sierra Minera of southeast Spain: *Journal of Environmental and Engineering Geophysics*, **14**, 63–76, doi: [10.2113/JEEG14.2.63](https://doi.org/10.2113/JEEG14.2.63).
- McNeill, J. D., 1980, *Electromagnetic terrain conductivity measurement at low induction numbers*: Technical Note 6, Geonics Limited.
- McKenna, S. P., B. S. Parkman, J. L. Perren, and R. J. McKenna, 2011, Response of an electromagnetic gradiometer to a subsurface wire: *IEEE Transactions on Geoscience and Remote Sensing*, **49**, 4944–4953, doi: [10.1109/TGRS.2011.2151867](https://doi.org/10.1109/TGRS.2011.2151867).
- Nabighian, M. N., and J. C. Macnae, 1991, Time domain electromagnetic prospecting methods, in M. N. Nabighian, ed., *Electromagnetic methods in applied geophysics: Applications, Parts A and B*, vol. 2, *Investigations in Geophysics 3*: SEG, 427–520.
- Patella, D., and A. Siniscalchi, 1994, Two-level magnetovariational measurements for the determination of underground resistivity distributions: *Geophysical Prospecting*, **42**, 417–444, doi: [10.1111/j.1365-2478.1994.tb00219.x](https://doi.org/10.1111/j.1365-2478.1994.tb00219.x).
- Peric, M., 1981, Exploration of Burundi nickeliferous laterites by electrical methods: *Geophysical Prospecting*, **29**, 274–287, doi: [10.1111/j.1365-2478.1981.tb00405.x](https://doi.org/10.1111/j.1365-2478.1981.tb00405.x).
- Price, A. T., 1949, The induction of electric currents in non uniform thin sheets and shells: *Quarterly Journal of Mechanics and Applied Mathematics*, **2**, 283–310, doi: [10.1093/qjmam/2.3.283](https://doi.org/10.1093/qjmam/2.3.283).
- Rutherford, J., T. Munday, J. Meyers, and M. Cooper, 2001, Relationship between regolith materials, petrophysical properties, hydrogeology and mineralisation at the Cawse Ni laterite deposits, Western Australia: Implications for exploring with airborne EM: *Exploration Geophysics*, **32**, 160–170, doi: [10.1071/EG01160](https://doi.org/10.1071/EG01160).
- Samouelian, A., I. Cousin, A. Tabbagh, A. Bruand, and G. Richard, 2005, Electrical resistivity survey in soil science: A review: *Soil & Tillage Research*, **83**, 173–193, doi: [10.1016/j.still.2004.10.004](https://doi.org/10.1016/j.still.2004.10.004).
- Sattel, D., and J. C. Macnae, 2001, The feasibility of electromagnetic gradiometer measurements: *Geophysical Prospecting*, **49**, 309–320, doi: [10.1046/j.1365-2478.2001.00244.x](https://doi.org/10.1046/j.1365-2478.2001.00244.x).
- Smith, R. S., 2000, The realizable resistive limit: A new concept for mapping geological features spanning a broad range of conductances: *Geophysics*, **65**, 1124–1127, doi: [10.1190/1.1444805](https://doi.org/10.1190/1.1444805).
- Smith, R. S., and A. P. Annan, 2000, Using an induction coil sensor to indirectly measure the B-field response in the bandwidth of the transient electromagnetic method: *Geophysics*, **65**, 1489–1494, doi: [10.1190/1.1444837](https://doi.org/10.1190/1.1444837).
- Smith, R. S., and G. F. West, 1987, Electromagnetic induction in an inhomogeneous conductive thin sheet: *Geophysics*, **52**, 1677–1688, doi: [10.1190/1.1442284](https://doi.org/10.1190/1.1442284).

- Swidinsky, A., and R. N. Edwards, 2009, The transient electromagnetic response of a resistive sheet: Straightforward but not trivial: *Geophysical Journal International*, **179**, 1488–1498, doi: [10.1111/j.1365-246X.2009.04393.x](https://doi.org/10.1111/j.1365-246X.2009.04393.x).
- Telford, W. M., L. P. Geldart, and R. E. Sheriff, 1990, *Applied geophysics*: Cambridge University Press.
- Vozoff, K., 1991, The magnetotelluric method, *in* M. N. Nabighian, ed., *Electromagnetic methods in applied geophysics: Applications, Parts A and B*, vol. 2, *Investigations in Geophysics 3*: SEG, 427–520.
- Walker, P., and Y. Lamontagne, 2006, Electromagnetic interpretation in complex geological environments: 76th Annual International Meeting, SEG, Expanded Abstracts, 1288–1292.
- West, G. F., J. C. Macnae, and Y. Lamontagne, 1984, A time-domain EM system measuring the step response of the ground: *Geophysics*, **49**, 1010–1026, doi: [10.1190/1.1441716](https://doi.org/10.1190/1.1441716).
- Xie, Y., Y. Xu, L. Yan, and R. Yang, 2005, Recovery of nickel, copper and cobalt from low-grade Ni-Cu sulfide tailings: *Hydrometallurgy*, **80**, 54–58, doi: [10.1016/j.hydromet.2005.07.005](https://doi.org/10.1016/j.hydromet.2005.07.005).